Functional ultrasound imaging of the spreading activity following optogenetic stimulation of the rat visual cortex

Authors: M. Provansal[1], G. Labernede[1], C. Joffrois[1], A. Rizkallah[1], R. Goulet[1], M. Valet[1], W. Deschamps[1], U. Ferrari[1], A. Chaffiol[1], D. Dalkara[1], J.A. Sahel[1,2,3], M. Tanter[4], S. Picaud[1], G. Gauvain*[1], F. Arcizet*[1].

- * Equal contribution

[1]Sorbonne Université, INSERM, CNRS, Institut de la Vision, F-75012 Paris, France; [2]Department of Ophthalmology, The University of Pittsburgh School of Medicine, Pittsburgh, PA 15213, United States; [3]Department of Ophthalmology and Vitreo-Retinal Diseases, Fondation Ophtalmologique Rothschild, F-75012 Paris, France; and [4]Physics for Medicine Paris, INSERM, CNRS, Ecole Supérieure de Physique et de Chimie Industrielles (ESPCI Paris), Paris Sciences et Lettres (PSL) Research University, 75012 Paris, France.

Optogenetic stimulation of the primary visual cortex (V1) is a promising therapy for sight restoration, but it remains unclear what total cerebral volume is activated after surface stimulation. In this study, we expressed the red-shifted opsin ChrimsonR in excitatory neurons within V1 in rats, and used the fine spatial resolution provided by functional ultrasound imaging (fUS) over the whole depth of the brain to investigate the brain response to focal surface stimulation. We observed optogenetic activation of a high proportion of the volume of V1. Extracellular recordings confirmed the neuronal origin of this activation. Moreover, neuronal responses were even located in deep layers under conditions of low irradiance, spreading to the LGN and V2, consistent with a normal visual information process. This study paves the way for the use of optogenetics for cortical therapies, and highlights the value of coupling fUS with optogenetics.

Introduction

29 Optogenetics has revolutionized investigation of the central nervous system[1], providing hope

30 for the treatment of a number of conditions, including deafness[2,3] or vision loss[4]. Optogenetic

31 therapy is already widely applied to retinal cells to restore vision for *in vivo* light application[5–

32 11], and is currently being assessed in two different clinical trials[12,13]. However, different

33 approaches, targeting cells other than those of the retina, are required for diseases causing

34 degeneration of the optic nerve (e.g. glaucoma) and for advanced retinal degeneration (late

35 AMD). For such conditions, direct stimulation of the primary visual cortex (V1) is a promising

36 alternative strategy. Indeed, high performance rates have been reported for the detection of

37 forms, with great accuracy, by blind human patients with cortical implants[14], and cortical

38 electrical prostheses have been shown to elicit visual percepts and to alter visual behavior in

39 nonhuman primates (NHP)[15]. Successes have been achieved with implantable devices, but

40 this approach nevertheless has a number of serious drawbacks: invasive surgery, signal

41 degradation over time, and a lack of cell-type specificity. In this respect, optogenetic therapy

42 stimulating V1 at the cortical surface could potentially afford similar benefits, but with less

43 invasive administration, stable expression over time and precise genetic targeting of the

44 appropriate cell population. Two of the key aspects of this strategy are the activation of

45 cortical layer IV neurons, as these are the first cells to receive visual information from the

46 visual thalamus[16] and the propagation of activity to other visual structures, which would favor

47 the generation of visual percepts.

48 Layer IV is located deep in the cortex (>1 mm in NHP). It is therefore a major challenge to

49 read and write neuronal activity, to demonstrate the efficacy of stimulation. Red-shifted

50 opsins are very good tools for neuronal stimulation, as they make it possible to use lower

51 light power to activate deeper neurons than blue-sensitive opsins, whilst also making it

52 possible to use higher light intensity safely[17–19]. Electrophysiological recordings can report

53 neuronal activity with unmatched spatiotemporal resolution, but over a very small spatial

54 area[20]. Conversely, techniques such as optical imaging and fMRI have been coupled with

55 optogenetics to report activity throughout the brain, but at the expense of a loss of both

2

56   spatial and temporal resolution[21,22]. Like fMRI, ultrafast functional ultrasound imaging (fUS)

57   can provide brain-sized maps of neurovascular activity changes, with a high spatiotemporal

58   resolution (100 μm x 100 μm, 1Hz) even in deep structures (up to 1.5 cm)[23]. This technique

59   has been used to investigate sensory processing in anesthetized[24], awake[24–26] and asleep[27]

60   rodents, and in behaving primates[28,29]. fUS imaging and electrophysiological recordings can,

61   therefore, be used to describe the dynamics of local neuronal activity accurately whilst

62   scanning neurovascular activity over the entire brain. We used these two techniques to

63   determine whether the optogenetic stimulation of V1 at the cortical surface could induce

64   neuronal activity even in deep cortical layers, and initiate the propagation of information to

65   other visual structures.

66   We show here that red light stimulation at the cortical surface can activate visual neurons

67   localized in deep cortical layers without triggering a thermal hemodynamic response and

68   toxicity. We were also able to follow the propagation of this information in other visual brain

69   structures (i.e. LGN and V2). More generally, this work shows that fUS imaging has the

70   potential to provide a clear, brain-wide mesoscopic view of the neuronal activities resulting

71   from optogenetic stimulation.

72

73   **Results**

74   **fUS imaging of V1 optogenetic activation in rats.** We used the optogenetic actuator

75   ChrimsonR for visual restoration in the cortex, because of its red-shifted opsin properties[17]

76   and because it was already being used for visual restoration in the primate retina[11] and had

77   given promising results in clinical trials[13]. We maximized the optogenetic activation of V1 by

78   using the CaMKII promoter to ensure expression limited to the excitatory neurons of V1.

79   Indeed, a ubiquitous promoter might lead to the silencing of pyramidal neurons through the

80   recruitment of inhibitory neurons. ChrimsonR was fused to the fluorescent reporter tdTomato

81   to facilitate the visualization of transfected areas. Following preliminary screening, we used

3

82   the AAV9-7m8 mutated viral capsid to express ChrimsonR in the V1 neurons of Long-Evans

83   rats (Fig. 1a). The mean rate of neuronal transfection was 5.5% over all cortical layers (Fig.

84   S1). ChrimsonR expression was not restricted to the soma, but spread to the axons and

85   dendrites (Fig. 1a). We assessed the efficacy of the optogenetic stimulation of V1 cortical

86   neurons, by using fUS imaging to measure brain activity in a large proportion of the brain:

87   from AP -3.5 mm to AP -8 mm, the zone in which most of the early visual system areas are

88   located. Activity in the cortical layers was assessed following either direct stimulation of the

89   contralateral eye with a white LED (58 mW.cm^{-2}), or stimulation at 595 nm delivered with an

90   optic fiber placed at the surface of the transfected or non-transfected V1 areas (7 mW, ~140

91   mW.mm^{-2} at the brain surface) (Fig. 1b). We chose to use durations and magnitudes of

92   parameters similar to those previously used[24,30] for stimulation of the eye or cortex (2 s at 4

93   Hz or 20 Hz for stimulation of the eye and cortex, respectively, separated by a 13 s period of

94   darkness. This cycle was performed 20 times). For eye stimulation (Fig. 1b, left), we first

95   imaged V1 with a single imaging plane at AP -7.5 mm and constructed an activation map

96   including only pixels displaying significant CBV (cerebral blood volume) responses (p<0.05

97   with Bonferroni-Holm correction, Wilcoxon signed-rank test, one-tailed, relative to baseline

98   activity). We detected strong activation in both the ipsilateral and contralateral superior

99   colliculi (SC) (ipsilateral, n=121/488 activated pixels; contralateral, n=134/421 activated

100   pixels), but almost no activation in the ipsilateral and contralateral V1 areas (ipsilateral,

101   n=8/634 activated pixels; contralateral, n=9/370 activated pixels). The lack of response in

102   both V1 areas and the strong signal in both SC may reflect the retinotectal nature of most

103   rodent retinal outputs[16] or an effect of anesthesia[31]. An increase in CBV was already clearly

104   visible on single-cycle responses (gray dashed lines), as illustrated for the significant pixel

105   (#14-92) in the ipsilateral V1 area (insert). Following direct stimulation of the contralateral

106   eye, the mean response (black curve) peaked 2 seconds after the two-second stimulation

107   represented by the patch in gray (mean: 19.8 ± 18.3%). For cortical stimulation (Fig. 1b,

108   center), we observed a broad activation of the ipsilateral V1 area (n=310/634 activated

109   pixels). The activation spread out of the V1 area at each border (medial and ventral) with V1

4

110   projections onto other visual areas. Single-cycle responses of the same example pixel

111   showed larger, less variable increases in CBV variation than for stimulation of the

112   contralateral eye (optogenetic, mean: 65.8 ± 32.6%, p<0.0001, Mann-Whitney). A previous

113   study showed that blue light delivery to the brain could itself generate non-specific changes

114   in CBV [30]. We therefore performed a control stimulation by locating the optic fiber at the

115   surface of the non-injected V1 area, which did not express ChrimsonR-tdT (Fig. 1b, right).

116   We used the same light stimulation parameters for this control as before. We detected no

117   significant CBV responses in the non-injected V1 area under such optogenetic stimulation

118   conditions.

119   We further characterized the V1 activation volume generated by contralateral eye stimulation

120   or by stimulation of the transfected V1 area, by imaging all the planes containing V1 (from AP

121   -6 to -8 mm, Fig. 1c-d). As shown in Fig. 1b, direct eye stimulation induced CBV responses

122   mostly in the SC areas, but very little activation was observed in the two V1 areas (mean:

123   0.05 ± 0.12%). Strikingly for the same animal shown (as shown in Fig. 1c), direct optogenetic

124   stimulation of the injected V1 area generated significantly stronger CBV responses, with a

125   mean active volume of 37% (range: 0.5 to 75.9%). The percentage mean active injected V1

126   area, over all animals, was higher for optogenetic cortical stimulation than for direct eye

127   stimulation (optogenetic, mean: 16.2 ± 17.8 %, Wilcoxon signed-rank test, one-tailed,

128   p=0.001, Fig. S1). Neurovascular activity and ChrimsonR expression were distributed

129   similarly along the AP axis and their amplitudes were correlated (Fig. 1d, Fig. S1). Again, our

130   control experiments demonstrated that direct optogenetic stimulation of a non-transfected

131   cortical area resulted in no activation. The findings for these control conditions indicate that

132   the parameters we used for optogenetic stimulation at the cortical surface did not generate

133   CBV variations in areas into which the virus was not injected (mean: 0 ± 0%). These

134   observations indicate that the optogenetic light stimulation used here does not trigger a

135   vascular response detectable by fUS imaging. Consequently, with fUS imaging, we were

136 able to visualize the entire volume of an optogenetically evoked response resulting from focal

137 stimulation within the primary visual cortex.

138 We then sought to confirm that the observed changes in blood volume following optogenetic

139 stimulation at the surface of V1 were indeed due to an increase in neuronal activity, and not

140 to indirect factors, such as heating. We therefore performed electrophysiological recordings

141 of V1 during the stimulation of the contralateral eye with white light (200 ms, 1 Hz, 100

142 cycles, 58 mW.cm^{-2}) or of the injected V1 area with light at 595 nm (200 ms, 1 Hz, 100

143 cycles, 140 mW.mm^{-2}). We used the Spyking Circus algorithm[32] to sort the multi-unit

144 recordings, to obtain single-cell responses. In total, we recorded a population of 171 neurons

145 from nine animals expressing ChrimsonR in V1. These neurons displayed several distinctive

146 patterns of activity under both direct eye and optogenetic stimulation conditions (Fig. 1e). We

147 plotted the spike density function (SDF) of four V1 neurons for both direct eye stimulation

148 (black lines) and optogenetic conditions (red lines), to highlight the diversity of these activity

149 patterns. Based on the profiles of visual and optogenetic responses, we classified neurons

150 into four different groups: neurons responding to both visual and optogenetic stimulation (V +

151 O neurons, n=13, 7.6%, Wilcoxon signed-rank test, two-tailed, p<0.01, between baseline: [-

152 100 0] ms, and stimulus presentation window: [0 200] ms), to visual stimulation only (V

153 neurons, n=20, 11.7%), to optogenetic stimulation only (O neurons, n=81, 47.4%), and non-

154 responsive neurons ('None' neurons, n=57, 33.3%). Most of the neurons responding to visual

155 stimulation displayed phasic responses, with an ON response occurring after the start of

156 stimulation followed, in some cases, by an OFF response. By contrast, the neurons

157 responding to optogenetic stimulation displayed a unique ON response. We characterized

158 the neuronal activation further, by comparing the onset latencies and durations of the V1

159 responses for both direct eye and optogenetic stimulation conditions, for V, O and V+O

160 neurons (n=109, Fig. 1f). As observed for the representative neurons shown in Fig. 2a, the

161 onset latencies of V1 responses were significantly shorter after optogenetic stimulation

162 (mean: 1.76 ± 3.14 ms, n=76 units) than after stimulation of the contralateral eye (mean:

6

163   41.24 ± 16.61 ms, *n*=33 units, Mann-Whitney, *p*<0.0001). These very short response

164   latencies for optogenetic stimulation are consistent with the direct activation of transfected

165   neuronal cell bodies, bypassing all retinal synapses, by contrast to natural visual signal

166   transmission. We also analyzed the duration of visual/optogenetic responses, to determine

167   whether V1 neurons presented transient or sustained activity, according to the type of

168   stimulation. For direct eye stimulation, the duration of neuronal responses was tuned on a

169   single ensemble, with a mean duration of activation of 28.09 ± 17.05 ms (*n*=33). By contrast,

170   in optogenetic conditions, two subgroups emerged: neurons displaying transient and

171   sustained responses. Based on these results, we defined two subsets of neurons: transient

172   (durations < 51 ms, *n*=33) and sustained (durations > 197 ms, *n*=22) neurons. The remaining

173   neurons (*n*=17) had intermediate response durations. The transient responses may result

174   from inhibitory cortical feedback from interneurons or a difference in voltage-gated channel

175   properties between neuronal subtypes leading to the silencing of these neurons. We found

176   no significant difference in the depth distribution of transient and sustained neurons (Fig. 1g),

177   revealing an absence of correlation between neuronal response patterns and potential

178   decreases in stimulus intensity with tissue depth; transient and sustained neurons were

179   recorded within the same cortical layers (L2/3 to L6), suggesting a direct activation of cortical

180   neurons by optogenetic stimulation at the cortical surface. We then assessed the specificity

181   of optogenetic activation, by performing electrophysiological recordings on naive animals. In

182   the animals in which no injection was performed (Fig. S1, *n*=3 animals), almost all the

183   recorded neurons (*n*=187/188) displayed a total absence of response to optogenetic

184   stimulation; the only responsive neuron had a very low response rate (3.89 Hz) relative to its

185   baseline activity (1.71 Hz, *p* = 0.0014). In this experiment, most neurons displayed a visual

186   response when the contralateral eye was stimulated (*n*=80/118), whereas another group of

187   neurons (*n*=37/118) did not respond to either visual or optogenetic stimulation. Thus, by

188   recording single-cell activities in transfected areas of V1, we were able to demonstrate that

189   optogenetic light stimulation at the surface of the cortex triggered both an increase in

190   cerebral blood volume, as shown by fUS imaging, and direct neuronal activation. We can

7

191   therefore conclude that the fUS variations we observed reflected the optogenetic activation of

192   V1 neurons. As in fUS imaging, we found that a larger number of neurons responded to

193   optogenetic stimulation than to visual stimulation (Fig. 1e), consistent with the broader

194   activation of areas in response to optogenetic stimulation than following direct contralateral

195   eye stimulation and fUS imaging.

Neuronal and neurovascular optogenetic sensitivity

197   As both single-cell recording and fUS imaging can be used to monitor optogenetic neuronal

198   activation, we decided to assess the sensitivities of these two approaches. We first imaged

199   the same single V1 plane (AP -7.5 mm) by fUS while optogenetically stimulating the surface

200   of the ChrimsonR-expressing V1 area with various irradiances (from 1.2 to 106 $mW.mm^{-2}$).

201   The size of the active volume within the injected V1 area increased with irradiance, with a

202   major increase between 36 $mW.mm^{-2}$ and 70 $mW.mm^{-2}$ and a slight decrease at 106

203    $mW.mm^{-2}$ (Fig. 2a). One also found that the contralateral SC was slightly activated at

204   irradiances above 1.2 $mW.mm^{-2}$. For each irradiance, we then calculated the mean CBV

205   variation over all significant pixels in the V1 area and over all trials (Fig. 2b, left panel). For

206   each animal, we normalized these values against those obtained for the highest irradiance

207   (106 $mW.mm^{-2)}$. Normalized CBV variation peaked 4 s after the start of stimulation. Peak

208   CBV values increased as a function of irradiance. No CBV variation was recorded for the

209   lowest irradiance (1.2 $mW.mm^{-2}$). Difference in peak CBV values relative to that for the

210   lowest irradiance tested started to become significant from 6 $mW.mm^{-2}$ onwards (1.2

211    $mW.mm^{-2}$, mean: 0 ± 0; 6 $mW.mm^{-2}$, mean: 0.36 ± 0.34, Wilcoxon signed-rank test, one-

212   tailed, $p<0.05$). For each irradiance, we then calculated the percentage normalized activated

213   ipsilateral V1 volume (Fig. 2b, right panel) in all animals (n=9). We again observed an

214   increase in the normalized active volume of V1 with irradiance. Difference with respect the

215   value obtained at the lowest irradiance became significant from 6 $mW.mm^{-2}$ onwards (1.2

216    $mW.mm^{-2}$, mean: 0 ± 0%; 6 $mW.mm^{-2}$, mean: 22.3 ± 39.0%, Wilcoxon signed-rank test, one-

217   tailed, $p<0.05$). We then investigated whether the variation of CBV responses observed with

218   irradiance was related to the number of neurons recruited. The SDF from a single-unit

219   example was determined for the different irradiances; the amplitude of the neuronal response

220   increased with irradiance from 8.2 ± Hz for 6 mW.mm^{-2} to 36.6 ± 73 Hz for 106 mW.mm^{-2}

221   (Fig. 2a). We generalized this analysis by plotting the cumulative distribution of the mean

222   maximal firing rates for each irradiance (Fig. 2c, left panel). The cumulative curves reached a

223   plateau for lower maximal firing rates with decreasing irradiance. We noted a significant

224   difference in distribution between 1.2 mW.mm^{-2} and irradiances of 6 mW.mm^{-2} and above

225   (1.2 mW.mm^{-2}, median: 0 Hz; 6 mW.mm^{-2}, 3.8 Hz, Kolmogorov-Smirnov test, $p<0.0001$),

226   demonstrating that electrophysiological recordings and fUS imaging had equivalent

227   sensitivities. Finally, in our total population of V1 neurons, the proportion of responsive

228   neurons increased with irradiance (from 28/92 units at 6 mW.mm^{-2} to 71/92 units at 106

229   mW.mm^{-2}, Fig. 2c, right panel). Interestingly, the depth distribution of the activated neurons

230   did not change with increasing irradiance (Fig. 2c, right panel). It was, therefore, possible to

231   activate neurons from deep cortical layers even at very low irradiances.

232   **Spread of optogenetic activation to downstream and upstream visual areas.** The results

233   described above relate to optogenetic activation in V1 with the optic fiber placed at the

234   surface of the primary visual cortex. We then investigated whether the activity initiated in V1

235   spread to other visual structures up- or downstream. This aspect is important for optogenetic

236   therapies for the restoration of cortical vision because it would demonstrate the propagation

237   of visual information favoring the generation of visual percepts. For the downstream pathway,

238   LGN terminals end in V1 at the depth of cortical layer IV, whereas cortical V1 layer VI sends

239   feedback connections to the LGN. We thus hypothesized that injecting AAV9-7m8-CaMKII-

240   ChrimsonR-tdT into V1 would increase ChrimsonR expression in at least one of these two

241   categories of fibers and that the optogenetic activation of V1 would lead to direct activation of

242   the LGN via LGN terminals in V1, or to an indirect activation of the LGN through feedback

243   connections in V1 cortical layer VI. Histological analyses confirmed that some ChrimsonR

244   expression occurred in the LGN, but we were unable to identify any ChrimsonR-expressing

9

245   cell bodies in the LGN, suggesting that only retrograde fibers originating from cortical V1

246   layer VI expressed this opsin (Fig. S2). We imaged the planes containing the LGN (AP -3.5

247   to AP -5.5 mm). Figure 3a shows the fUS imaging planes at AP -5 mm for the direct eye and

248   optogenetic stimulation conditions. We noted a slight activation of the visual cortex following

249   visual stimulation (see Fig. 1b), and a strong activation of the ipsilateral LGN (n=85/225

250   active pixels) when the contralateral eye was stimulated with the white LED, suggesting that

251   this kind of stimulation was more appropriate for LGN and SC activations than for the visual

252   cortex. Indeed, in the 11 animals (Fig. 3b), the mean percentage of the LGN volume visually

253   activated was 20.5 ± 13.7% which is much greater than the volume activation obtained for V1

254   (less than 1%). When the injected V1 surface was stimulated with the optic fiber (Fig. 3a),

255   CBV responses increased significantly in the ipsilateral LGN, but with a much smaller

256   number of activated pixels (n=12/225 pixels) than for visual stimulation. We also performed a

257   control optogenetic stimulation, in which we stimulated the non-injected V1 area. We

258   observed no activation of the ipsilateral LGN, confirming that, on stimulation of the injected

259   hemisphere, ipsilateral LGN activation was due to optogenetic activation of LGN terminals in

260   V1 or feedback from the V1 area (Fig. S2). In the 11 animals tested, the active LGN volumes

261   for visual stimulation were larger than those for optogenetic stimulation (visual, mean: 20.5 ±

262   13.7%; optogenetic, mean: 6.5 ± 12.3%, Wilcoxon signed-rank test, p=0.0068). In addition,

263   for the five animals tested by optogenetic stimulation of the non-transfected V1 area, we

264   detected no significant responsive pixels (Fig. 3b, mean: 0 ± 0%, n=5 animals). We also

265   performed single-cell recordings in the LGN, to demonstrate that the neurovascular

266   activations imaged by fUS in the LGN coincided with the activation of LGN neurons (Fig. 3c).

267   We recorded a total of 153 neurons in the LGN. Only two units responded to both visual and

268   optogenetic stimulation; seven units were responsive only to optogenetic stimulation, and 40

269   units were responsive only to visual stimulation (n=7 animals). The vast majority of LGN

270   neurons were unresponsive to both types of stimulation. The distribution of onset latencies

271   following direct eye stimulation was broader for LGN than for V1 single units (Fig. 3d, mean:

272   47.88 ± 23.55 ms, n=42 units, and see Fig. 1f). This may reflect the recording of both cells

10

273   activated by retinal ganglion cells and cells retrogradely activated by the V1 area, which have

274   higher latencies. Following optogenetic stimulation at the surface of the V1 area, the onset

275   latencies for LGN neurons were shorter than those following visual stimulation (mean: 9.86 ±

276   4.95 ms, *n*=7 units, Mann-Whitney, *p*<0.05). However, these response latencies were greater

277   than those recorded in V1 (*n*=42 units. Mann-Whitney, *p*<0.0001, see Fig 1f for V1 units).

278   This result suggests that the optogenetically activated LGN single units recorded here were

279   activated indirectly, by retrograde fibers from V1 cortical layer VI, as suggested by the

280   histological data.

281   We also investigated whether V1 optogenetic stimulation could spread to the direct upstream

282   visual area toward which V1 projects: the V2 area. We obtained fUS activation maps in

283   different imaging planes (AP -6 to AP -8 mm) in which the entire V2 area was present after

284   either direct stimulation of the contralateral eye or optogenetic stimulation at the surface of

285   the V1 area. We show representative activation maps from single imaging planes (AP -8.5

286   mm) in Figure 4a. Visual stimulation of the contralateral eye led to almost no activation of the

287   V2 area on the same side as the injected V1. By contrast, optogenetic stimulation of the

288   transfected V1 area led to a stronger activation of the ipsilateral V2, mostly within the ventral

289   part of V2. As previously reported, within the different imaging planes, we also observed

290   strong activation in the lower parts of V1 and V2 containing the axons. We next quantified the

291   active volume over all imaging planes for the V2 area, for all 10 animals (Fig. 4b). As for the

292   V1 area, visual stimulation resulted in only weak activation of V2 (mean: 0.2 ± 0.3% of

293   activated volume). Averaged activation volumes were significantly larger for optogenetic

294   stimulation than for visual stimulation (mean: 5.6 ± 8.0% activated volume, *n*=10 animals,

295   Wilcoxon signed-rank test, one-tailed, *p*<0.05). Control stimulation of the non-injected V1

296   area confirmed the specificity of the spread of optogenetic activation from V1 to V2, as no

297   activation was observed in the contralateral V2 area (Fig. 4b, Fig. S2).

298   Electrophysiological recordings within V2 confirmed that the fUS variations we observed in

299   V2 were consistent with direct neuronal activation (Fig. 4c). We recorded V2 single units

11

300   responding to visual and optogenetic stimulation. As previously described, we characterized

301   the onset latency of these neurons, comparing the values obtained with those for V1 single

302   units (Fig. 4d). Similar visual latencies were recorded for V1 and V2 single units (V1, mean:

303   41.24 ± 16.61 ms, n=33 units (see Fig. 1f); V2, mean: 39.43 ± 9.557 ms, n=14 units).

304   Interestingly, optogenetic onset latencies were higher for V2 single units than for V1 (V1,

305   mean: 1.76 ± 3.14 ms, n=76 units. V2, mean: 62.78 ± 77.44 ms, n=9 units, Mann-Whitney,

306   p<0.0001), suggesting that these neurons were activated indirectly by ChrimsonR-expressing

307   V1 neurons. Two V2 neurons presented particularly long optogenetic ON latencies, possibly

308   due to a difference in the microcircuits involved. We checked that this variability did not bias

309   the latency delay for V2 and V1 neurons after optogenetic stimulation, by performing the

310   same statistical test on a V2 data set restricted to the remaining seven fast V2 units. The

311   difference in ON latency between V1 neurons and these fast V2 neurons was conserved

312   (fast V2 units, mean: 12.2 ± 9.5 ms, n=7 units, Mann-Whitney, p<0.0001), suggesting that all

313   V2 neurons were activated indirectly after the onset of stimulation. This conclusion is

314   supported by the lack of ChrimsonR expression in V2 on brain slices from the animals used

315   to record these single units. However, these V2 latencies were shorter than V2 latencies for

316   natural eye stimulation, demonstrating that they were genuinely produced by V1 optogenetic

317   activation.

318

319   **Discussion**

320   **Coupling of optogenetics with fUS**

321   In this study, we demonstrate that optogenetic activation can be detected by fUS imaging.

322   Rungta and colleagues[30] indicated that blue light from the tip of the optic fiber *per se* could

323   induce neurovascular responses in naïve mice, at irradiances higher than 2 mW ~ 18

324   mW.mm^{-2}. Another recent study reported hemodynamic responses following blue light

325   illumination of the retrosplenial cortex in Thy-ChR2 mice or the illumination of specific

326   neuronal subpopulations of the superior colliculus in other transgenic lines[26]. The authors

327   explained that they used a lower light power and irradiance (0.3 mW ~1.5 mW.mm^{-2}) to

328   prevent non-specific activation. By contrast, we used an AAV-mediated strategy to express

329   ChrimsonR in V1 neurons, resulting in a lower density of opsin-expressing cells than in

330   transgenic mice lines[33]. This generalizes the possibility of recording neurovascular

331   optogenetic activation due to a small number of transfected neurons. Moreover, we show

332   here that stimulation of the control non-injected hemisphere does not induce a vascular

333   response, thereby demonstrating the specificity of ChrimsonR-elicited optogenetic activity.

334   Single-cell recordings confirmed the neuronal optogenetic activation correlated with these

335   CBV variations. We also used a higher wavelength (595 nm) for illumination than Rungta and

336   coworkers, but with comparable values of power and irradiance. These results indicate that

337   red light can be used even at high power, in protocols combining the optogenetic activation

338   of red-shifted opsins and fUS imaging. Importantly, electrophysiological recordings from the

339   control animals showed no neuronal activation, suggesting negligible thermal effects with the

340   use of 595 nm light under the parameters used here. Indeed, we included these parameters

341   in the heat propagation model of Stujenske[34], and recorded a very local (<1 mm-diameter

342   sphere from the tip of the optic fiber) increase in temperature, by 0.2°C, which is too small to

343   alter neuronal firing rates. Finally, we characterized the dose-response dependence of our

344   recorded optogenetic activations. We obtained equivalent sensitivities for optogenetic

345   responses measured by fUS imaging and by electrophysiological recordings.

346   The use of fUS imaging to analyze optogenetic responses has the advantage that it could

347   potentially provide a mesoscopic view of the activated area. Unlike electrophysiological

348   recordings, which extract information very locally[20], and calcium imaging, which is dependent

349   on both expression of the calcium indicator and the penetration of blue light through the

350   tissue[35], it can display information at a brain-wide spatial scale. The coupling of fMRI with

351   optogenetics meets these criteria, but with a lower spatial resolution[21,22,36] (of the order of a

352   millimeter per pixel). By contrast, fUS imaging can detect brain activity at a submesoscopic

353   resolution (100 x 100 μm²), with less cumbersome equipment than for fMRI.

354   **Spread of the activity**

355   We found that optogenetic neurovascular activation was well correlated with ChrimsonR

356   expression in the AP axis. We also noted that optogenetic V1 stimulation spread beyond the

357   borders of V1, as indicated by the activation of both the LGN and V2 on both fUS and

358   electrophysiology. This spread of activity may be due to fibers located at the base of V1,

359   connected to the LGN and expressing ChrimsonR (Fig. S1). These fibers may generate the

360   neurovascular activity detected ventrally to V1 on our activation maps. Furthermore, the

361   mean neuronal transfection rate was 5.5% in the coronal plane displaying the highest

362   fluorescence signal, whereas a larger volume of V1 was activated in this plane. A first

363   explanation for this may be the spread of neuronal activation to other V1 cells, although we

364   recorded a rather homogeneous set of short-onset latencies. Alternatively, neurovascular

365   activations may be broader *per se* than neuronal responses. Some studies of rat olfactory

366   bulb glomeruli have provided evidence of a close overlap between capillary blood flow and

367   neuronal activity[37], whereas others have reported a mismatch between the areas of

368   neurovascular and neuronal activation[38,39]. Specifically for V1, a lack of correlation between

369   BOLD signals and spiking activity has been observed in cats[40], and a lack of correlation

370   between single-vessel hemodynamic responses and calcium imaging signals has been found

371   in cats and rats[41]. Importantly, we show here that the neurovascular and neuronal activities

372   initiated in V1 spread to the LGN and V2. This propagation of visual information is important

373   for optogenetic cortical vision restoration therapy, because it favors the generation of visual

374   percepts.

375   **Cortical visual restoration**

376   We detected neurovascular and neuronal responses, even at low irradiance (6 mW.mm^{-2}),

377   with no modification of the depth distribution of the activated neurons. One recent study[42]

14

378   reported that the stimulation of deep V1 layers (>1.5 mm) in non-human primates with

379   electrical prostheses elicited behavioral responses. Our ability to activate neurons in deep

380   cortical layers highlights the potential value of red-shifted opsin ChrimsonR for optogenetic

381   cortical vision restoration strategies. A key element of visual restoration is the induction of

382   neuronal responses with characteristics matching those resulting from a natural visual

383   stimulus[5–11]. We show here that the firing rates induced by optogenetic stimulation were

384   similar to those induced by visual stimulation. Optogenetically activated neurons had very

385   short latencies, of the order of 1-2 ms. Theoretically, this is sufficient for the encoding of

386   natural images into optogenetic stimulations at a temporal resolution matching the resolution

387   of the natural visual signal. Moreover, those optogenetic onset latencies were quite

388   homogeneous, despite being obtained for neurons located in different layers. These results

389   demonstrate that we can induce a signal that does not lose its temporal resolution with

390   depth.

391   Finally, the feasibility of inducing visual percepts by optogenetic cortical vision restoration

392   remains to be demonstrated. In species with a more complex hierarchical organization of

393   cortical visual areas, such as nonhuman primates, a few studies have shown behavioral

394   effects due to the optogenetic stimulation of higher visual areas. Jazayeri[43] and coworkers

395   reported that saccades following fixation tasks were shifted towards the receptive field of the

396   region of V1 optogenetically activated following the fixation point offset. Ju[44] and coworkers

397   demonstrated the successful detection of optogenetic percepts in a saccade task. Our ability

398   to detect a spread of activity from V1 to other visual areas is consistent with these behavioral

399   studies indicating perception. Here, we used a single optic fiber for optogenetic stimulation.

400   Replacing this device with a more complex stimulation system, such as arrays of micro-

401   LEDs, might make it possible to generate percepts more complex than phosphenes and to

402   develop discrimination behavioral tasks to assess their perception.

403

404   **Materials and methods**

Animals

All animal experiments and procedures were approved by the Local Animal Ethics Committee (registration number 2018032911282465) and performed in accordance with European Directive 2010/63/UE. We used wild-type male Long-Evans rats (Janvier Laboratories), nine weeks old at the time of viral injection. Rats were maintained under a reverse 12-hour light/12-hour dark cycle, with ad libitum access to food and water, except during surgery and electrophysiological recordings.

AAV production

The AAV9-7m8-CaMKII-ChrimsonR-tdT vector was packaged as previously described, by the triple transfection method, and purified by iodixanol gradient ultracentrifugation[45]. The AAV9-7m8-CaMKII-ChrimsonR-tdT vector was titered by qPCR with SYBR Green[46] (Thermo Fisher Scientific). The titer used in this study was 4.39×10^{12} vg.mL^{-1}.

Immunostaining and confocal imaging

Following electrophysiological recordings, rats were euthanized, and their brains were extracted and fixed by overnight incubation in 4% paraformaldehyde (100496, Sigma-Aldrich) at 4°C. Brains were then cryoprotected in 30% sucrose (84097, Sigma-Aldrich) and 50 µm sagittal slices were cut with a microtome (HM450, Microm). The slices with the most intense tdT fluorescence from each brain were selected for further immunohistochemistry and imaging. Cryosections were permeabilized by incubation with 0.5% Triton X-100 in PBS for 1 h at room temperature and were then incubated in blocking buffer (PBS + 1% BSA + 0.1% Tween 20) for 1 hour at room temperature. Samples were incubated overnight at 4°C with monoclonal anti-NeuN antibody (1:500; Mouse, MAB377, Merck Millipore), in a 50% dilution of blocking buffer + 0.5% Triton X-100. Secondary antibodies conjugated with Alexa Fluor dyes (1:500; Molecular Probes) and DAPI (1:1000, D9542, Merck Millipore), were incubated with the samples for 1 hour at room temperature. An Olympus FV1000 laser-scanning confocal microscope with a 20x or 40x objective (UPLSAPO 20XO, NA: 0.85) was used to acquire images of brain sections.

Viral injections

Viral injections were performed in aseptic conditions with a digital small-animal stereotaxic instrument (David Kopf Instruments). Ear bars were covered with xylocaine to ensure that the animals felt no pain. Rats were anesthetized in a sealed box containing gaseous isoflurane (5%), and maintained under anesthesia in the stereotaxic frame (25% ketamine, 10%

16

437 medetomidine and 65% saline injected intraperitoneally) for the entire surgical procedure,
438 and animal body temperature was maintained at 37°C with a heating pad. Buprenorphine
439 was injected subcutaneously to reduce inflammation, and Lubrithal was applied to the eyes
440 to prevent them from drying out. Xylocaine, 70% ethanol and Vetedine were applied
441 successively to the scalp before incision, to minimize pain and maintain sterile conditions.
442 Cranial sutures were cleaned to remove connective tissue, by applying H_2O_2, to facilitate
443 localization of the injection coordinates. We injected a total volume of 1.2 μL of viral
444 suspension unilaterally into rates, via two injection tracks, at a flow rate of 50-75 nL/min, with
445 a 5 or 10 μL microsyringe (Hamilton) equipped with a microinjector (Sutter Instrument) and
446 controller (World Precision Instruments). The coordinates for viral injection were +2.8 / +3.2
447 mm from midline (M-L axis), -6.5 / -7.5 mm from Bregma (A-P axis) and 1.6-1.35-1.1 mm
448 ventral to the skull surface (D-V axis), based on the 2004 edition of the Paxinos and Franklin
449 rat brain atlas. Viral efflux was prevented by leaving the needle in a 1.8 mm ventral position
450 for two minutes before beginning the injection, with a three-minute interval left between
451 injections before complete withdrawal of the needle from the cortex. After surgery, rats were
452 brought round from anesthesia with a subcutaneous injection of Antisédan (0.15 mL).

453 *In vivo* electrophysiological recordings

454 Bilateral craniotomies were performed with a digital small-animal stereotaxic instrument
455 (David Kopf Instruments), at least 30 days after viral injection, to allow time for opsin
456 expression. Ear bars were covered with xylocaine to prevent pain. Rats were anesthetized in
457 a sealed box containing gaseous isoflurane (5%) and maintained under anesthesia in the
458 stereotaxic frame (25% ketamine, 10% medetomidine and 65% saline injected
459 intraperitoneally) for the entire surgical procedure, and electrophysiological recordings were
460 taken with body temperature maintained at 37°C with a heating pad. Buprenorphine was
461 injected subcutaneously to reduce inflammation, and Lubrithal was applied to the eyes to
462 prevent them from drying out. Cranial sutures were cleaned to remove connective tissue, by
463 applying H_2O_2, to reveal the injection tracks. Parietal bones were removed by drilling
464 rectangular flaps and gently moving the bone away from the dura mater, exposing the cortex
465 from 3 to 8.5 mm from Bregma (A-P axis), to cover the injection tracks. The dura was then
466 gently removed. During drilling, the skull was regularly cooled with PBS, and once the cortex
467 was exposed, it was protected from dehydration by the regular application of cortex buffer.
468 After surgery, electrophysiological recordings were performed with 16-channel electrodes
469 (A1x16-5 mm-50-703-OA16LP) coupled with a 400 μm-core fiber (Thorlabs M79L005 Fiber
470 Cable, MM, 400 μm 0.39NA, FC/PC to 1.25 mm ferrule, 0.5 m) at various positions close to
471 the injection sites. Electrophysiological data were acquired with MC RACK software. For

472 visual stimulation, a white LED (Thorlabs MNWHL4 Mounted LED, 5V, 60 mW/cm^2) was

473 placed 15 cm in front of the eye on the contralateral side of the cranial window.

474 **Acquisition protocol for electrophysiological recordings**

475 For optogenetic stimulation, we connected the optic fiber (reference above) to a light source

476 (Thorlabs M595F2 (fiber coupled LED @595 nm), Ø400 µm, 150 µW/cm^2) delivering light at

477 the ChrimsonR excitation wavelength (595 nm). We targeted the transfected region of V1 by

478 imaging tdT fluorescence with a Micron IV imaging microscope (Phoenix Research

479 Laboratories) before recordings. The fiber was placed on the surface of the cortex while the

480 electrode was inserted in the tissue. Both stimulations consisted of 100 repeats of 200 ms

481 flashes at 1 Hz. The onset of the flashes was aligned with electrophysiological data, with

482 Clampex 9.2 software. We used several different irradiances of light at 595 nm in this study.

483 Power at the fiber tip was measured with a power meter (Thorlabs, PM100D), by placing the

484 fiber tip in contact with the sensor. The irradiance corresponding to each power was

485 calculated as previously described[30].

486

Irradiance (mW.mm^{-2})	Power (mW)
142	7.1
140	7.0
106	5.3
70	3.5
36	1.8
14	0.7
6	0.3
1.2	0.06

487 Table 1: 595 nm light irradiances and powers used in this study

488 **Spike sorting**

18

489 Offline spike sorting of the electrophysiological recordings (linear 16-channel electrodes) was
490 performed with the SpyKING CIRCUS package[32]. Raw data were first high-pass filtered (>
491 300 Hz) and spikes were detected when a filtered voltage trace crossed the threshold.
492 Automatic cluster extraction was performed and candidate clusters were curated. Refractory
493 period violations (< 2 ms, >1% violation) and noisy spike shapes led to cluster deletion. Spike
494 templates with coordinated refractory periods in the cross-correlogram together with similar
495 waveforms led to the merging of cluster pairs.

496 **Electrophysiological data analysis**

497 All electrophysiological data were extracted and analyzed with a custom-made Matlab script.
498 Responsive units were defined as those displaying a significant difference in neuronal activity
499 between the pre-stimulation period (averaged 100 ms before stimulus onset) and the
500 stimulation interval (averaged 200 ms following stimulus onset, Wilcoxon signed-rank test,
501 $p<0.01$). For each unit, responses are represented as the spike density function (SDF), which
502 was calculated from the mean peristimulus time histogram (PSTH, bin size: 1 ms, 100 trials)
503 smoothed with a Gaussian filter (2 ms SD).

504 **Calculation of latencies and response durations**

505 The latency of the units displaying activation was defined as the first time point at which the
506 SDF crossed the value of the baseline plus 2SD and remained higher than this value for at
507 least 10 ms. Conversely, the offset of activation was defined as the first time point after
508 latency that the SDF crossed back below the value of the baseline plus 2SD and remained
509 lower than this value for at least 10 ms. Not all active neurons from a given population met
510 these criteria, accounting for the slight difference between the number of active neurons and
511 the number of latencies presented here.

512 **Generation of functional ultrasound images**

513 fUS imaging was performed as previously described[24], with a linear ultrasound probe (128
514 elements, 15 MHz, 110 µm pitch and 8 mm elevation focus, Vermon; Tour, France) driven by
515 an ultrafast ultrasound scanner (Aixplorer, Supersonic Imagine; Aix-en-Provence, France).

516 **Acquisition protocol for fUS imaging**

517 3D fUS acquisitions were performed after craniotomy and electrophysiological recordings, as
518 previously described. When optogenetic responses were observed, the position of the optic
519 fiber on the surface of the cortex was kept unchanged until control acquisitions were
520 performed, in which the fiber was moved to the other hemisphere. The cortex buffer on the

521 surface of the cortex dried out, and 1 cm^3 of ultrasound coupling gel was placed between the
522 cortex and the linear ultrasound probe. Acquisition protocols consisted of 20 stimulation
523 blocks, each consisting of 13 s of rest followed by 2 s of stimulation. For visual stimulation,
524 the white LED used for electrophysiological recordings was kept in the same position, and
525 the 2 s stimulation consisted of eight repeats of 125 ms flashes at 4 Hz. For optogenetic
526 stimulation, the 2 s stimulation consisted of 40 repeats of 25 ms flashes at 20 Hz.
527 Acquisitions were performed on coronal planes from 3 mm to 8.5 mm from Bregma (AP
528 axis), with a 0.5 mm increment corresponding to the thickness of the imaging plane.

529 **Building activation maps**

530 For each pixel, we averaged, for each block, the intensity of Doppler power at baseline (2 s
531 before stimulus onset) and during a response window (4 s after stimulus onset). The signals
532 were then compared in one-tailed Wilcoxon signed-rank tests. Only pixels with p-values <
533 4.03×10^{-6} (corresponding to a global p-value < 0.05 with Bonferroni correction) were
534 considered significant. On the maps, CBV during the response window is presented as a
535 percentage of the baseline value. Region of interest (ROI) as V1, V2, SC and LGN were
536 determined for each imaging plane, based on the Matt Gaidica rat brain atlas.
537
538

539 **References**

540 1. Deisseroth, K. Optogenetics: 10 years of microbial opsins in neuroscience. *Nat. Neurosci.* **18**,

541 1213–1225 (2015).

542 2. Wrobel, C. *et al.* Optogenetic stimulation of cochlear neurons activates the auditory pathway and

543 restores auditory-driven behavior in deaf adult gerbils. *Sci. Transl. Med.* **10**, (2018).

544 3. Dieter, A., Keppeler, D. & Moser, T. Towards the optical cochlear implant: optogenetic approaches

545 for hearing restoration. *EMBO Mol. Med.* **12**, e11618 (2020).

546 4. Roska, B. & Sahel, J.-A. Restoring vision. *Nature* **557**, 359–367 (2018).

547 5. Bi, A. *et al.* Ectopic Expression of a Microbial-Type Rhodopsin Restores Visual Responses in Mice

548 with Photoreceptor Degeneration. *Neuron* **50**, 23 (2006).

549   6. Lagali, P. *et al.* Light-activated channels targeted to ON bipolar cells restore visual function in

550   retinal degeneration. *Nature neuroscience* vol. 11 https://pubmed.ncbi.nlm.nih.gov/18432197/

551   (2008).

552   7. Gaub, B. M. *et al.* Restoration of visual function by expression of a light-gated mammalian ion

553   channel in retinal ganglion cells or ON-bipolar cells. *Proc. Natl. Acad. Sci. U. S. A.* **111**, E5574–

554   E5583 (2014).

555   8. Khabou, H. *et al.* Noninvasive gene delivery to foveal cones for vision restoration. *JCI Insight* **3**,

556   (2018).

557   9. Sengupta, A. *et al.* Red-shifted channelrhodopsin stimulation restores light responses in blind

558   mice, macaque retina, and human retina. *EMBO Mol. Med.* **8**, 1248–1264 (2016).

559   10.   Chaffiol, A. *et al.* A New Promoter Allows Optogenetic Vision Restoration with Enhanced

560   Sensitivity in Macaque Retina. *Mol. Ther.* **25**, 2546–2560 (2017).

561   11.   Gauvain, G. *et al.* Optogenetic therapy: High spatiotemporal resolution and pattern

562   recognition compatible with vision restoration in non-human primates. *bioRxiv*

563   2020.05.17.100230 (2020) doi:10.1101/2020.05.17.100230.

564   12.   Allergan. *Phase I/IIa, Open-Label, Dose-Escalation Study of Safety and Tolerability of*

565   *Intravitreal RST-001 in Patients With Advanced Retinitis Pigmentosa (RP)*.

566   https://clinicaltrials.gov/ct2/show/NCT02556736 (2020).

567   13.   GenSight Biologics. *A Phase 1/2a, Open-Label, Non-Randomized, Dose-Escalation Study to*

568   *Evaluate the Safety and Tolerability of GS030 in Subjects With Retinitis Pigmentosa*.

569   https://clinicaltrials.gov/ct2/show/NCT03326336 (2020).

570   14.   Beauchamp, M. S. *et al.* Dynamic Stimulation of Visual Cortex Produces Form Vision in

571   Sighted and Blind Humans. *Cell* **181**, 774-783.e5 (2020).

572   15.   Bosking, W. H., Beauchamp, M. S. & Yoshor, D. Electrical Stimulation of Visual Cortex:

573   Relevance for the Development of Visual Cortical Prosthetics. *Annu. Rev. Vis. Sci.* **3**, 141–166

574   (2017).

575   16.   Seabrook, T. A., Burbridge, T. J., Crair, M. C. & Huberman, A. D. Architecture, Function, and

576   Assembly of the Mouse Visual System. *Annu. Rev. Neurosci.* **40**, 499–538 (2017).

577   17.   Klapoetke, N. C. *et al.* Independent optical excitation of distinct neural populations. *Nat.*

578   *Methods* **11**, 338–346 (2014).

579   18.   Mager, T. *et al.* High frequency neural spiking and auditory signaling by ultrafast red-shifted

580   optogenetics. *Nat. Commun.* **9**, 1750 (2018).

581   19.   Marshel, J. H. *et al.* Cortical layer-specific critical dynamics triggering perception. *Science* **365**,

582   (2019).

583   20.   Buzsáki, G., Anastassiou, C. A. & Koch, C. The origin of extracellular fields and currents —

584   EEG, ECoG, LFP and spikes. *Nat. Rev. Neurosci.* **13**, 407–420 (2012).

585   21.   Liang, Z. *et al.* Mapping the Functional Network of Medial Prefrontal Cortex by Combining

586   Optogenetics and fMRI in Awake Rats. *NeuroImage* **117**, 114–123 (2015).

587   22.   Chen, X. *et al.* Mapping optogenetically-driven single-vessel fMRI with concurrent neuronal

588   calcium recordings in the rat hippocampus. *Nat. Commun.* **10**, (2019).

589   23.   Macé, E. *et al.* Functional ultrasound imaging of the brain. *Nat. Methods* **8**, 662–664 (2011).

590   24.   Gesnik, M. *et al.* 3D functional ultrasound imaging of the cerebral visual system in rodents.

591   *Neuroimage* **149**, 267–274 (2017).

592   25.   Macé, É. *et al.* Whole-Brain Functional Ultrasound Imaging Reveals Brain Modules for

593   Visuomotor Integration. *Neuron* **100**, 1241-1251.e7 (2018).

594   26.   Brunner, C. *et al.* A Platform for Brain-wide Volumetric Functional Ultrasound Imaging and

595   Analysis of Circuit Dynamics in Awake Mice. *Neuron* **108**, 861-875.e7 (2020).

596   27.   Bergel, A., Deffieux, T., Demené, C., Tanter, M. & Cohen, I. Local hippocampal fast gamma

597   rhythms precede brain-wide hyperemic patterns during spontaneous rodent REM sleep. *Nat.*

598   *Commun.* **9**, (2018).

599   28.   Dizeux, A. *et al.* Functional ultrasound imaging of the brain reveals propagation of task-

600   related brain activity in behaving primates. *Nat. Commun.* **10**, (2019).

22

601   29.   Blaize, K. *et al.* Functional ultrasound imaging of deep visual cortex in awake nonhuman

602   primates. *Proc. Natl. Acad. Sci. U. S. A.* **117**, 14453–14463 (2020).

603   30.   Rungta, R. L., Osmanski, B.-F., Boido, D., Tanter, M. & Charpak, S. Light controls cerebral

604   blood flow in naive animals. *Nat. Commun.* **8**, 14191 (2017).

605   31.   Gao, Y.-R. *et al.* Time to wake up: Studying neurovascular coupling and brain-wide circuit

606   function in the un-anesthetized animal. *NeuroImage* **153**, 382–398 (2017).

607   32.   Yger, P. *et al.* A spike sorting toolbox for up to thousands of electrodes validated with ground

608   truth recordings in vitro and in vivo. *eLife* **7**,.

609   33.   Arenkiel, B. R. *et al.* In vivo light-induced activation of neural circuitry in transgenic mice

610   expressing channelrhodopsin-2. *Neuron* **54**, 205–218 (2007).

611   34.   Stujenske, J. M., Spellman, T. & Gordon, J. A. Modeling the Spatiotemporal Dynamics of Light

612   and Heat Propagation for In Vivo Optogenetics. *Cell Rep.* **12**, 525–534 (2015).

613   35.   Emiliani, V., Cohen, A. E., Deisseroth, K. & Häusser, M. All-Optical Interrogation of Neural

614   Circuits. *J. Neurosci.* **35**, 13917–13926 (2015).

615   36.   Gerits, A. *et al.* Optogenetically-induced behavioral and functional network changes in

616   primates. *Curr. Biol. CB* **22**, 1722–1726 (2012).

617   37.   Chaigneau, E., Oheim, M., Audinat, E. & Charpak, S. Two-photon imaging of capillary blood

618   flow in olfactory bulb glomeruli. *Proc. Natl. Acad. Sci.* **100**, 13081–13086 (2003).

619   38.   Iadecola, C., Yang, G., Ebner, T. J. & Chen, G. Local and propagated vascular responses

620   evoked by focal synaptic activity in cerebellar cortex. *J. Neurophysiol.* **78**, 651–659 (1997).

621   39.   Iadecola, C. The neurovascular unit coming of age: a journey through neurovascular coupling

622   in health and disease. *Neuron* **96**, 17–42 (2017).

623   40.   Kayser, C., Kim, M., Ugurbil, K., Kim, D.-S. & König, P. A Comparison of Hemodynamic and

624   Neural Responses in Cat Visual Cortex Using Complex Stimuli. *Cereb. Cortex* **14**, 881–891 (2004).

625   41.   O'Herron, P. *et al.* Neural correlates of single-vessel haemodynamic responses in vivo. *Nature*

626   **534**, 378–382 (2016).

627   42.   Chen, X., Wang, F., Fernandez, E. & Roelfsema, P. R. Shape perception via a high-channel-

628   count neuroprosthesis in monkey visual cortex. *Science* **370**, 1191–1196 (2020).

629   43.   Jazayeri, M., Lindbloom-Brown, Z. & Horwitz, G. D. Saccadic eye movements evoked by

630   optogenetic activation of primate V1. *Nat. Neurosci.* **15**, 1368–1370 (2012).

631   44.   Ju, N., Jiang, R., Macknik, S. L., Martinez-Conde, S. & Tang, S. Long-term all-optical

632   interrogation of cortical neurons in awake-behaving nonhuman primates. *PLoS Biol.* **16**, e2005839

633   (2018).

634   45.   Choi, V. W., Asokan, A., Haberman, R. A. & Samulski, R. J. Production of recombinant adeno-

635   associated viral vectors. *Curr. Protoc. Hum. Genet.* **Chapter 12**, Unit 12.9 (2007).

636   46.   Aurnhammer, C. *et al.* Universal real-time PCR for the detection and quantification of adeno-

637   associated virus serotype 2-derived inverted terminal repeat sequences. *Hum. Gene Ther.*

638   *Methods* **23**, 18–28 (2012).

639

640 Acknowledgments

646 Competing financial interests

647   M.T. is cofounder and S.P. and M.T. are shareholders of ICONEUS. D.D. and S.P. are consultants for
648   Gensight Biologics.

649 Author contributions

650   M.P., S.P., J-A.S., M.T., G.G., and F.A. designed the study; M.P. and D.D. designed viral vectors; M.P.
651   and W.D. produced viral vectors; M.P., G.L., A.R., R.G. and M.V. performed intracortical injections;
652   M.P., G.L. and C.J. performed electrophysiological recordings and fUS acquisitions; G.L. performed
653   histological experiments; M.P., U.F., A.C., G.G., F.A. and S.P. analyzed data; M.P., G.G. and F.A.
654   constructed the figures; M.P., A.C., G.G., F.A. and S.P. wrote the manuscript.
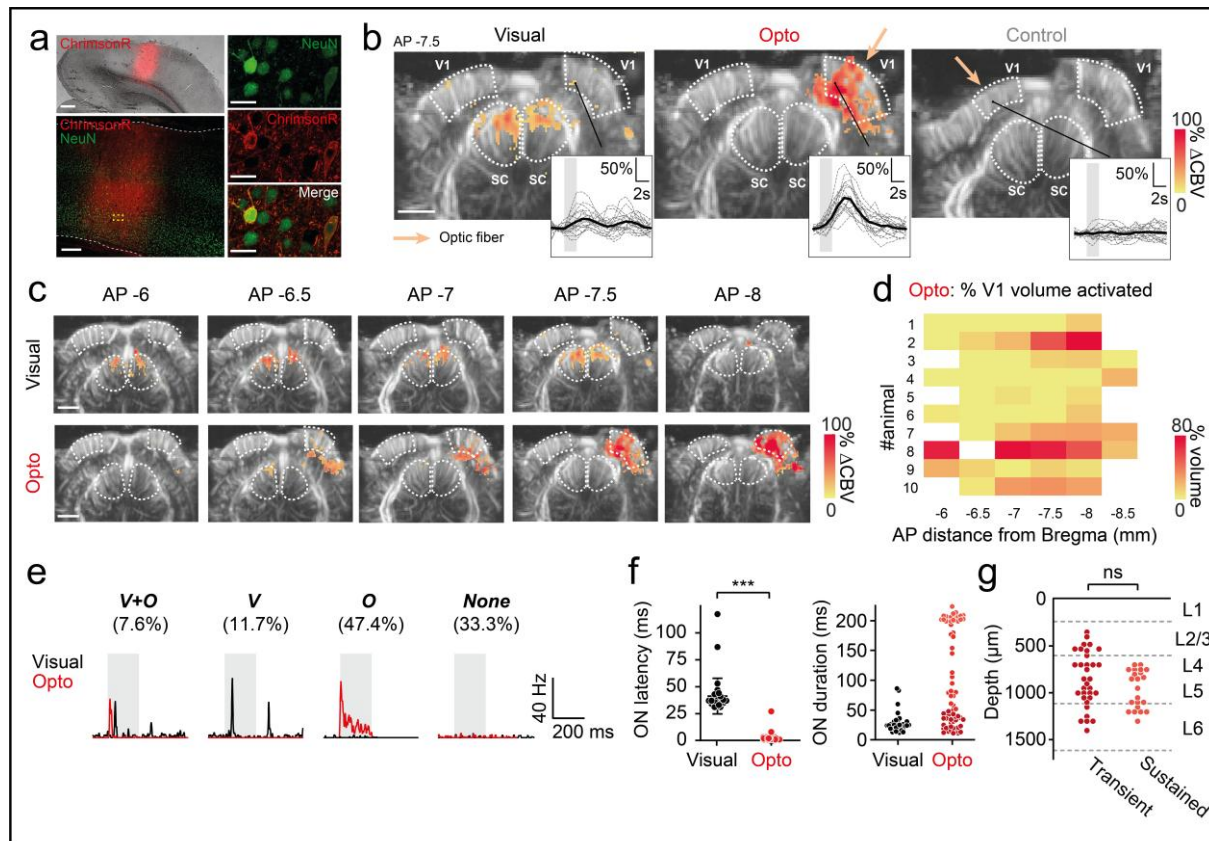
655

656

Figure 1 | V1 neurovascular and neuronal activations resulting from cortical surface stimulation in rats. (a) Left: 2.5x imaging (top) and 20x confocal imaging of a brain section showing the localization of ChrimsonR in V1. White dashed lines delimit the cortical surface and border between V1 and the white matter. Right: close-up (40x) of the area delimited by the yellow lines in the previous image, showing two ChrimsonR-expressing neurons. Scale bars: 500 μm, 200 μm, 20 μm. (b) fUS activation maps obtained after visual stimulation of the contralateral eye (left), optogenetic stimulation of the ipsilateral V1 area expressing ChrimsonR (middle) and control optogenetic stimulation of the uninjected contralateral V1 area (right), from a single imaging plane (AP -7.5 mm) from the same animal. White dashed lines delimit the V1 and SC areas. Colored pixels indicate significant CBV variation (Wilcoxon signed-rank test with Bonferroni-Holm correction). Right insets: patterns of single-pixel activation. Gray lines represent single-trial activity (n=20) and the black line represents the mean CBV variation. Colored patches indicate light stimulation (duration: 2 s) (c) fUS activation maps for visual and optogenetic activation, for all imaging planes (AP -6 mm to AP -8 mm) in which V1 (delimited by white dashed lines) is present, from the same animal (animal #2). (d) Left: percentage of V1 activated during optogenetic stimulation for each fUS imaging plane, for all animals (n=10). Right: AP distribution of the ChrimsonR expression area on brain sections. (e) Spike density function (SDF) of typical V1 single units during visual (black lines) or optogenetic (red lines) activation. Four subpopulations of neurons were identified: double-responsive (n_{V+O}=13), responsive to the visual (n_V=20) or optogenetic stimulus only (n_O=81), non-responsive (n_{None}=57). (f) Left: ON response latencies for visual (n=33 units) and optogenetic (n=76 units) stimulation (Mann-Whitney, p<0.0001). Right: ON response durations for visual (n=33 units) and optogenetic stimulation (n=72 units). (g)

679   Depth profile of transient (ON duration<51 ms, n=33 units) and sustained (ON duration>197 ms, n=22

680   units) neurons activated by optogenetics. (c-d) Scale bar: 2 mm. The irradiance used for optogenetic

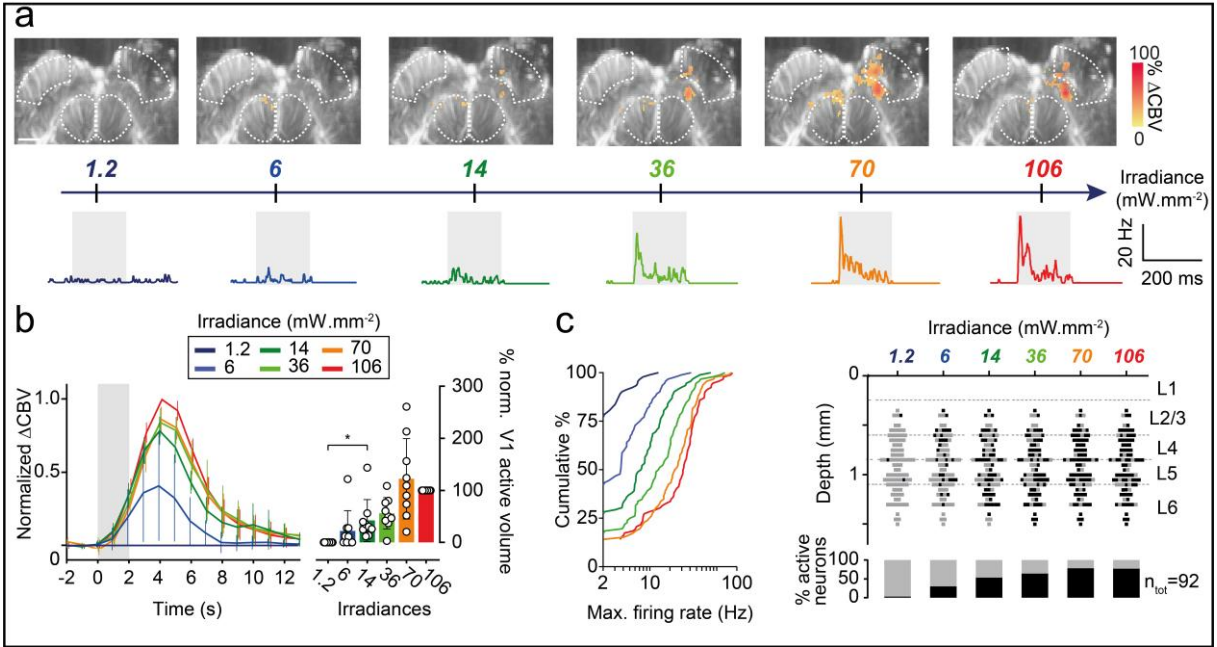681   and control stimulation was 140 mW.mm^{-2}.

682

683

684   **Figure 2 | Neuronal and neurovascular optogenetic sensitivity.** (a) Top: fUS activation maps of a

685   single imaging plane (AP -7.5 mm) from animal #4 at different irradiances. Scale bar: 2 mm. White

686   dashed lines delimit the V1 and SC areas. Bottom: SDF from a typical V1 single unit during

687   optogenetic stimulation for 200 ms (gray patch) at different irradiances. (b) Left panel: mean CBV

688   variation over all animals (n=9) for each irradiance. of the values for each animal were normalized

689   against those obtained at 106 mW.mm^{-2}. Error bars represent the standard deviation. The colored

690   patch corresponds to the 2 s optogenetic stimulation. Right panel: normalized active volumes of the

691   ipsilateral V1 area for each irradiance. Open circles are individual values, bars represent the mean

692   and the standard deviation (n=9 animals, Wilcoxon signed-rank test, one-tailed, p<0.05). (c) Left:

693   cumulative distribution of the mean maximal firing rates of all recorded V1 single units (n=92) during

694   optogenetic stimulation, for each irradiance. Right panel, top: depth profile of V1 single units activated

695   (black squares) or not (gray squares) by the optogenetic stimulation, for each irradiance (n=92 single

696   units). Bottom: percentage of active (black) and non-responsive (gray) neurons for each set of

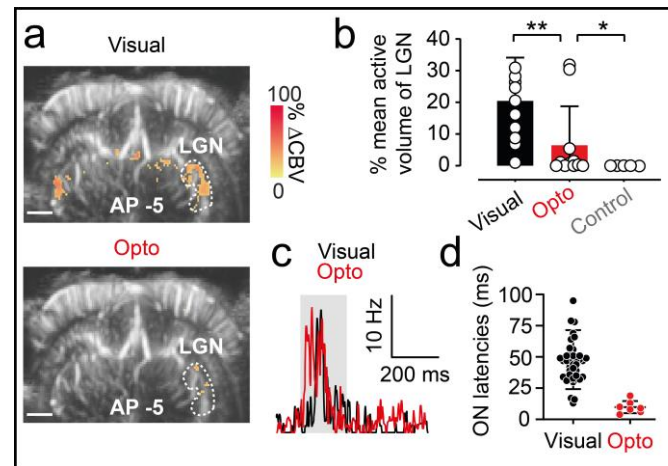697   conditions.

698

26

699

Figure 3 | Spread of optogenetic activation to the LGN. (a) fUS activation maps obtained during visual stimulation of the contralateral eye (top) and optogenetic stimulation of the ChrimsonR-expressing ipsilateral V1 area (bottom) from a single imaging plane in which the LGN is present (AP -5 mm) from the same animal. White dashed lines delimit the ipsilateral LGN. Scale bar: 2 mm. (b) Percentage active volume of the LGN after visual, optogenetic or control stimulation. For both visual and optogenetic stimulations, we show the volumes of the LGN ipsilateral to the injection, whereas, for control stimulations, the volume of the contralateral LGN is shown. Open circles represent mean values over all imaging planes for each animal (visual and optogenetic stimulation, n=11, Wilcoxon signed-rank test, one-tailed, p=0.0068, n=5 for control, Mann-Whitney test, one-tailed, p=0.0288), bars represent the mean for all animals. (c) SDF of a typical LGN single unit responding to visual (black line) and optogenetic (red line) stimulation of the ipsilateral V1 area. (d) ON latencies of V1 and LGN single-unit responses to visual (V1, n=33 units, LGN, n=42 units) or optogenetic stimulation of V1 (V1, n=29 units, LGN, n=7 units. Mann-Whitney test, p<0.05). The irradiance used for optogenetic and control stimulation was 142 mW.mm^{-2}.
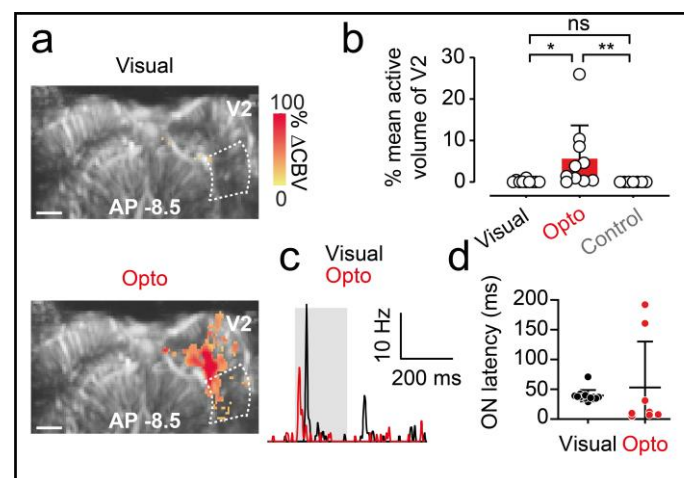
714

715

Figure 4 | Spread of the optogenetic activation to V2. (a) fUS activation maps obtained during visual stimulation of the contralateral eye (top) and optogenetic stimulation of the ChrimsonR-

27

718   expressing ipsilateral V1 area (bottom) and control stimulation of the uninjected contralateral area from

719   a single imaging plane (AP -7.5 mm) containing the V2 area. White dashed lines delimit the ipsilateral

720   V2 area. Scale bar: 2 mm. (b) Percentage active volume of V2 after visual, optogenetic or control

721   stimulation. For both visual and optogenetic stimulation, we show the volumes of V2 ipsilateral to the

722   injection, whereas, for the control, we shown the volume of the contralateral V2. Open circles

723   represent mean values over all imaging planes for each animal (visual and optogenetic, n=1, Wilcoxon

724   signed-rank test, one-tailed, p=0.002, n=7 for control, Mann-Whitney test, one-tailed, p=0.0004), bars

725   represent the mean over all animals. (c) SDF of a typical V2 single unit responding to visual (black

726   line) and optogenetic (red line) stimulation of the ipsilateral V1 area. (d) ON latencies of V1 and V2

727   single-unit responses to visual (V1, n=33 units, V2, n=14 units) or optogenetic stimulation of V1 (V1,

728   n=76 units, V2, n=8 units). The irradiance used for optogenetic and control stimulation was 140

729   mW.mm^{-2}.